JOURNAL OF CATALYSIS **179,** 72–89 (1998)
ARTICLE NO. CA982198

Complete Oxidation of CO, Ethanol, and Ethyl Acetate over Copper Oxide Supported on Titania and Ceria Modified Titania

Per-Olof Larsson* and Arne Andersson†,[1]

*Perstorp Catalysts, Perstorp AB, S-284 80 Perstorp, Sweden; and †Department of Chemical Engineering II, University of Lund, Chemical Center, P.O. Box 124, S-221 00 Lund, Sweden

Received February 23, 1998; revised June 3, 1998; accepted June 5, 1998

Titania and titania modified with 3 and 12 μmol Ce/m^2 surface area of the titania were prepared and were used as supports for copper oxide. Preparations with 3 and 12 μmol CuO_x/m^2 surface area of the support were tested for the combustion of CO, ethyl acetate, and ethanol. The results show that the Ce-doped titania surface is good as support for CuO_x and that the cerium not only enhances the activity of the copper species, but also stabilises the surface area of the TiO_2 support in the presence of copper oxide. Additions of Al, K, and La are also found to stabilise the TiO_2 support but, compared with Ce, these elements do not to the same extent enhance the activity of the copper species. Acetaldehyde is observed to be an intermediate in the combustion of both ethanol and ethyl acetate over Cu-Ce-Ti-O catalysts. Since acetaldehyde is more harmful than any of the reactants and also is photochemically active, it is in applications important to assure that the combustion is complete. Cu-Ce-Ti-O catalysts show good performance not only for feeds without water vapour, but also for humid feeds. Although the concentrations of intermediates are affected by the addition of water, there is little effect on the temperature required for obtaining complete conversion to carbon dioxide and water. Characterisation with XRD, FT-Raman, TPR, and XPS indicates that the dispersed copper species are in the form of patches or a bidimensional layer which interacts with the surface of the support. When the content of cerium and copper is low, other types of dispersed copper species are present, which possibly are monomers or dimers. The copper species are predominantly Cu^{2+} species.

INTRODUCTION

Volatile organic compounds (VOCs) include all organic compounds that exist in the gaseous state in ambient air. Offensive odours and toxic air emissions as well as the formation of ground-level ozone and photochemical smog are environmental problems which are related to emissions of VOCs. To reduce the environmental impact of these emissions and be able to fulfil established goals regarding the reduction of VOCs, the legislation which already partly has been introduced will become more stringent and broader. Anthropogenic emissions of VOCs are emitted from stationary, mobile, and diffuse sources, e.g. from processes utilising organic solvents, coatings, and fuels. In some segments of the printing industry the dominating waste gas contains a mixture of ethyl acetate and ethanol in humid air. One competitive method to reduce these emissions is catalytic incineration (1–4).

Complete oxidation of ethanol over catalysts has mainly been studied regarding control of the emissions from ethanol-fuelled vehicles (5–9). According to McCabe *et al.* (5, 6) and Yu Yao (7), Pt/Al_2O_3 catalysts are in general slightly more active than base metal oxide catalysts on the same volume basis (same GHSV). However, base metal oxide catalysts may be an alternative due to the fact that these are much cheaper than Pt, allowing a higher catalyst load. A higher loading of active phase in the metal oxide bed also makes the catalyst less sensitive than the platinum catalyst to nonselective poisoning. Deactivation due to nonselective poisoning, fouling, or masking is common in applications for stationary emission control (10). Rajesh *et al.* (8) and Yu Yao (7) have found CuO/Al_2O_3 to be the most active base metal oxide catalyst for the complete oxidation of ethanol.

Complete oxidation of ethyl acetate over platinum on alumina has been studied by Sawyer *et al.* (11), who concluded that the platinum mainly produced complete oxidation products. Additionally, partial oxidation products like ethanol, acetic acid, and ethyl ether were observed due to reaction over the bare alumina support.

The probability of forming partial oxidation products that are more harmful than the original organic compounds is very high during the complete oxidation of oxygenated compounds like, e.g. ethanol and ethyl acetate. However, compared with applications for vehicles, an advantage in catalytic incineration after stationary sources is the possibility to keep the catalyst temperature high enough for the complete oxidation to form CO_2 and H_2O. In applications water vapour is always present in the gas, and it is

[1] Corresponding author.

0021-9517/98 $25.00

important to study whether the performance of the catalyst and the by-product formation are affected by water vapour. In most cases, the waste gas contains a mixture with several organic compounds. Consequently, it is important to investigate if mixtures behave differently from single-component systems. According to Spivey (12), few systematic studies concerning complete oxidation of VOC mixtures have been reported.

In a previous publication (13) we found that dispersed copper oxide on titania is active for the complete oxidation of CO and toluene. However, a problem was the accelerated sintering of the titania in the presence of copper. In the present work we have tried to stabilise the CuO_x/TiO_2 catalyst with different elements (Al, K, Ce, La), using the oxidation of CO as a test reaction. Alumina (14) and potassium oxide (15) have previously been found to stabilise TiO_2, and cerium oxide and lanthanum oxide (16, 17) have, for example, been shown to stabilise alumina. Due to the fact that we observed both stabilisation and increased CO oxidation activity when ceria was added, another part of our work concerns a more detailed investigation of the CuO_x-CeO_x/TiO_2 system for the oxidation of CO and, especially, for the complete oxidation of ethanol and ethyl acetate as well as their mixture.

EXPERIMENTAL

Catalyst Preparation

The used TiO_2 support (XT 25376) was supplied by Norton and consists of 1.6 mm extrudates (TiO_2, anatase) with a specific surface area of 173 m^2/g and a pore volume of 0.37 cm^3/g. Due to thermal instability of TiO_2 with such high surface area, the extrudates were calcined at 600°C for 72 h before further use. This pretreatment gave a TiO_2 support with a specific surface area of 42 m^2/g and a pore volume of 0.33 cm^3/g. The extrudates were then cut and sieved to a median length of about 5 mm. The diameter was still 1.6 mm after the calcination.

The CuO_x/TiO_2 catalysts were prepared by impregnating the precalcined TiO_2 support with an aqueous solution of copper nitrate, giving a loading of either 3 μmol CuO_x/m^2 or 12 μmol CuO_x/m^2. The impregnation was performed by first evacuating the TiO_2 extrudates for 10 min at 50 torr. The copper nitrate solution was then added at the low pressure, and subsequently the pressure was increased to atmospheric pressure (760 torr). The extrudates remained immersed for 1 h in the copper nitrate solution. After the impregnation the extrudates were dried and calcined in the following sequence. First the sample was dried at 60°C for 14 h and then at 120°C for another 6 h. From 120°C the temperature was increased with 10°C/min up to 300°C, where it was held for 1 h. In this step most of the nitrate decomposed to nitrogen oxides. Finally, the temperature was increased by 10°C/min up to 550°C, where the extrudates were calcined for 6 h. The prepared CuO_x/TiO_2 catalysts with a copper loading of 3 μmol Cu/m^2 and 12 μmol Cu/m^2 are denoted Cu3Ti and Cu12Ti, respectively.

For the preparation of the CuO_x-CeO_x/TiO_2 catalysts, first, CeO_x/TiO_2 without copper was prepared using the same procedure as was described above for preparation of the CuO_x/TiO_2 catalysts, with the exception that a cerium nitrate solution was used, instead of the copper nitrate solution. After the preparation and calcination of the CeO_x/TiO_2 extrudates, impregnation with copper nitrate solution was performed followed by drying and calcination using the same procedure as for the CuO_x/TiO_2 catalysts. The prepared CuO_x-CeO_x/TiO_2 catalysts are denoted Cu*y*Ce*z*Ti, where *y* and *z* are the loading of CuO_x and CeO_x, respectively, expressed in μmol/m^2 surface area of the precalcined TiO_2 support, i.e., Cu3Ce3Ti, Cu12Ce3Ti, Cu3Ce12Ti, and Cu12Ce12Ti.

The CuO_x (12 μmol/m^2)-KO_x (12 μmol/m^2)/TiO_2, CuO_x (12 μmol/m^2)-AlO_x (12 μmol/m^2)/TiO_2, and CuO_x (12 μmol/m^2)-LaO_x (12 μmol/m^2)/TiO_2 catalysts for the stabilisation tests were prepared by the same procedure as was used to prepare the Cu12Ce12Ti catalyst, starting from nitrate solutions with either potassium, aluminium, or lanthanum. These preparations are denoted Cu12K12Ti, Cu12Al12Ti, and Cu12La12Ti.

The amounts of loaded cations in the catalysts are all based on the specific surface area of the precalcined TiO_2 support (42 m^2/g). Thus, the decrease in surface area in sequential impregnations has not been taken into account. Values on the specific surface area of the prepared samples are given in Table 1 and Fig. 1.

TABLE 1

Specific Surface Area, Pore Size Distribution, and Pore Volume of the Different Samples

Sample	BET surface area[a] (m^2/g)		Pore size distribution[b] (Å)		Pore volume[c] (cm^3/g)	Water uptake (cm^3/g)
TiO_2, as obtained	173	(173)	25 - 300	(35, 150)	0.40	0.37
TiO_2, pre-calcined	42	(42)	150 - 450	(280)	0.31	0.33
Cu3Ti	37	(37)	175 - 450	(290)	0.31	
Cu12Ti	25	(26)	200 - 600	(350)	0.27	
Ce3Ti	40	(41)	150 - 450	(280)	0.32	
Cu3Ce3Ti	37	(38)	150 - 450	(290)	0.31	
Cu12Ce3Ti	33	(35)	150 - 500	(290)	0.29	
Ce12Ti	36	(39)	150 - 450	(280)	0.28	
Cu3Ce12Ti	35	(38)	150 - 450	(290)	0.28	
Cu12Ce12Ti	33	(37)	150 - 450	(280)	0.26	

[a] The BET surface area in m^2/g of catalyst and, within brackets, in m^2/g of support.

[b] The pore diameter at the distribution maximum is given within brackets.

[c] The desorption pore volume for the 17–3000 Å range of pore diameters.

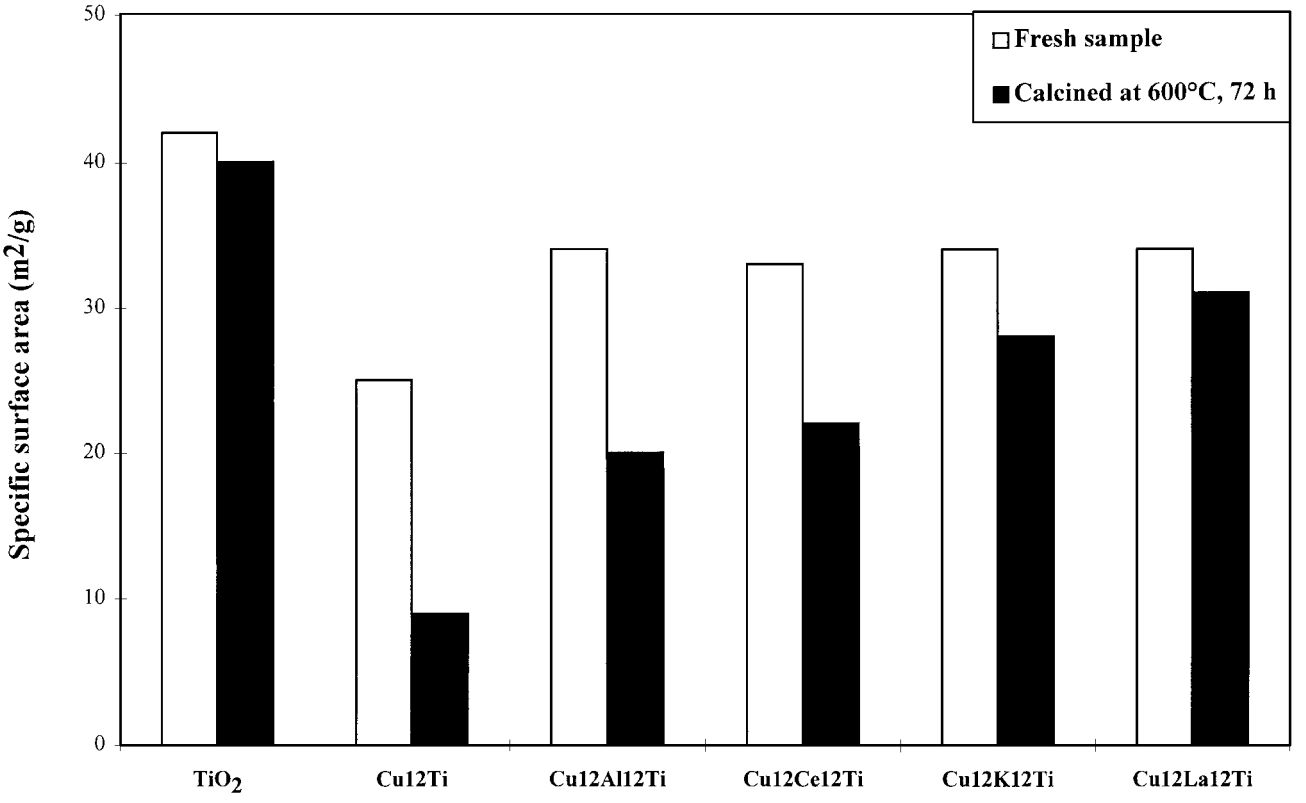

FIG. 1. Specific surface area of freshly prepared samples and of the same samples after an extra heat treatment at 600°C for 72 h. Data are shown for the pure TiO_2 support and 12 μmol CuO_x/m^2 loaded on pure TiO_2 and TiO_2 stabilised with 12 μmol/m^2 of either Al, Ce, K, or La.

Catalytic Tests

The catalytic tests were performed at a gas hourly space velocity (GHSV) of 20,000 h^{-1}. A fixed volume of catalyst, 120 ml, was always loaded in the cylindrical (44 mm in diameter) and adiabatic stainless steel reactor. The total feed was 40 liters/min (STP) and was passed through an electric preheater before entering the reactor. The temperature was measured with two thermocouples, which were located 15 mm in front of and 5 mm after the catalyst bed, respectively. The flow of dry air, free of carbon dioxide, and the flow of CO were fed using mass flow controllers (Brooks). Liquid ethyl acetate, ethanol, and water were injected with liquid pumps (Alitea) into the stream of air, passing heated evaporators before reaching the preheater. To obtain better adiabatic conditions, the reactor was surrounded with insulation, which was heated to the same temperature as the inlet gas to the reactor. All pipes were heated to prevent condensation.

CO_2 and CO in the inlet and outlet gas were continuously analysed with an IR instrument (Fuji electronic, ZRF IR-analyser, 0–2000 ppm CO_2 and 0.000–1.000% CO) by passing a flow of 0.5 l/min of the gas through, first, a condenser (Insat AG, JCP-FE) and, then, through the IR-instrument. Ethyl acetate, ethanol, and other possible organic by-products were continuously analysed on-line with an FID-detector (Bernath Atomic, model 3006) by passing a flow of 1.5 liters/min of the inlet or outlet gas from the reactor to the FID-analyser. A gas chromatograph (Varian 3400), which was equipped with an FID detector and a 3 m × 1/8 inch packed Haysep Q column, was operated at 180°C to allow separation of ethanol, acetaldehyde, acetic acid, and ethyl acetate. No other organic compounds were detected.

The catalytic measurements were performed at steady state conditions in steps of 25°C from 50°C and above for the oxidation of CO and from 175°C and above for the oxidation of ethyl acetate, ethanol, and a mixture of these. When steady state conditions had been reached, the hydrocarbon and/or the CO and CO_2 concentrations, together with the inlet and outlet reactor temperatures were continuously recorded during at least 10 min when sampling after the reactor, and during 10 min when sampling in front of the reactor. When using GC analysis this time was prolonged, and at least two analyses were performed for each temperature. Finally, average values were calculated.

Test of ethyl acetate oxidation in an empty reactor showed that the yields to CO_2, ethanol, acetaldehyde, and acetic acid all were below 1% between 175–275°C. In a corresponding ethanol oxidation test, the yields to CO_2, ethyl acetate, and acetic acid were below 1%. In this case, however, due to partial oxidation in the stainless steel reactor

system the yield to acetaldehyde was around 5% at 175°C, and it increased with increasing temperature. At 275°C the yield to acetaldehyde was around 18%. For the oxidation of the mixture of ethyl acetate and ethanol in an empty reactor, the same results were observed as for the single component systems. Almost no ethyl acetate was converted, although a small amount of ethanol was oxidised to give acetaldehyde.

Characterisation of Catalysts

The specific surface area (BET), pore volume, and pore size distribution were measured with a Micromeritics ASAP 2400 instrument using adsorption of N_2 at the temperature of liquid nitrogen. Pore volume and pore size distribution in the range 17–3000 Å were calculated with the method of Barrett, Joyner, and Halenda (18). All samples were degassed at 350°C for 16 h before analysis.

X-ray diffraction (XRD) analysis was carried out on a Seifert XRD 3000 TT diffractometer using monochromatic CuKα radiation (50 kV/30 mA). The scanning range was 2.5–45° (Θ) with a step size of 0.01° and a step time of 1.0 s. Compound identification was accomplished by comparison with JCPDS data (19). The measurements were performed on ground samples with particle diameters <150 μm using a rotating sample holder.

Temperature programmed reduction (TPR) was performed on a Micromeritics TPD/TPR 2900 instrument. The temperature was increased from 30°C to 1000°C with a heating rate of 10°C/min. The reducing gas was 5 vol% H_2 in N_2 and a flow rate of 50 ml/min was used. The water produced during the reduction process was condensed in a cold trap at about −90°C. The 4-mm quartz tube reactor was loaded with 0.142 g sample with particle sizes in the range 150–355 μm.

FT-Raman spectra were recorded on a Bruker IFS 66/FRA 106 instrument equipped with a low-power diode pumped Nd : YAG laser and a liquid nitrogen cooled high sensitive germanium diode detector. The laser power was 100 mW, the resolution was 4 cm^{-1}, and 1000 scans were recorded for every spectrum. The samples were ground to particle diameters <150 μm before analysis and were loaded in a quartz tube, 5 mm in diameter, which was used as sample holder (180° backscattering).

X-ray photoelectron spectroscopy (XPS) spectra were recorded on a Kratos XSAM 800 spectrometer. Al Kα (1486.6 eV) and Mg Kα (1253.6 eV) anodes operating at an accelerating voltage of 13 kV and a current of 19 mA were used as radiation source. The used pass energy was 80 eV at low magnification. The residual pressure inside the spectrometer was 10^{-8} torr, or, lower. Charging effects were corrected for by adjusting the main C 1s peak to a position of 285.0 eV, and the analysed samples had been ground to particle diameters <150 μm. Due to photoreduction of dispersed copper oxide and cerium oxide in the spectrometer, single scan spectra were recorded first for the Cu 2p and Ce 3d regions. A complete analysis of all regions took 18 min. The regions were analysed both with the Mg anode and the Al anode due to interference in the Cu 2p region from Auger lines when the Al anode was used, and in the Ce 3d region when the Mg anode was used. Due to the photoreduction, fresh samples were used every time the anode was switched. Wide scan recordings were performed after analysis of the regions to assure that no unexpected elements were present. For quantitative purposes instrumental sensitivity factors, 1.8 for Ti 2p, 6.3 for Cu 2p, and 10.0 for Ce 3d, were used together with linear baselines.

RESULTS

Stabilisation of CuO_x/TiO_2

Figure 1 shows the specific surface area for unstabilised and stabilised CuO_x/TiO_2 samples both as freshly prepared and after an extra heat treatment in air at 600°C for 72 h. The extra heat treatment of the TiO_2 support gives almost no decrease in surface area, which is a consequence of the support in a previous step once being precalcined at 600°C for 72 h (see Experimental). However, in the presence of copper the TiO_2 support shows accelerated sintering. For the fresh Cu12Ti sample, which after the deposition with copper had been calcined for 6 h at 550°C, the specific surface area is 25 m^2/g to be compared with 42 m^2/g for the support. After the extra heat treatment at 600°C the corresponding value is only 9 m^2/g. Figure 1 shows surface area values around 34 m^2/g for the fresh stabilised samples. Compared with the pure TiO_2 support, these values are smaller, which is due to the mass contribution from copper and the stabilising agent, as well as some pore clogging. After the heat treatment at 600°C the specific surface area of the stabilised samples has in all cases decreased, although not as much as for the unstabilised Cu12Ti. The data in Fig. 1 clearly show that the effect of stabilisation increases in the order Al < Ce < K < La.

In order to evaluate how the stabilising cation affects the activity, the catalysts were tested for the complete oxidation of 0.2 vol% CO in air. Figure 2 shows the results. Addition of Al, K, or La to the Cu12Ti catalyst hardly affects the activity. However, the addition of Ce increases the CO oxidation activity considerably. Over the Cu12Ce12Ti catalyst, compared with the Cu12Ti catalyst, it is possible to obtain the same conversion level at about 50°C lower inlet temperature. Due to the fact that ceria both stabilises the surface area and gives enhanced activity to the catalyst for the oxidation of CO, the CuO_x-CeO_x/TiO_2 system was chosen for more detailed characterisation and investigation regarding complete oxidation.

Catalytic Tests

Complete oxidation of 0.2 vol% CO in air. Figure 3 shows the results for the combustion of 0.2 vol% CO in air

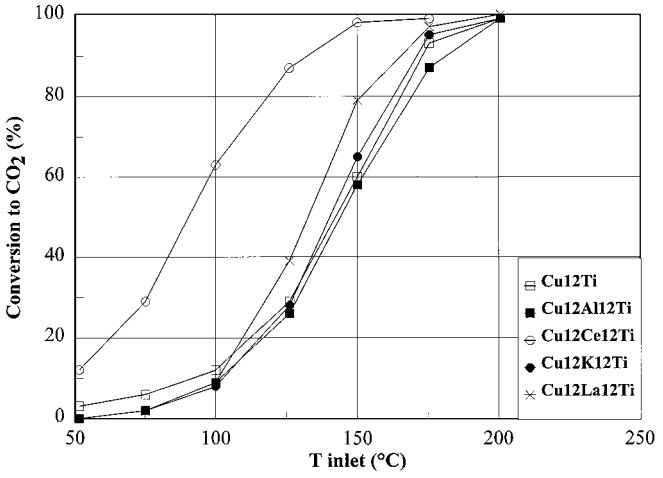

FIG. 2. Comparison of unstabilised and Al-, Ce-, K-, and La-stabilised CuO_x/TiO_2 for the complete oxidation of 0.2 vol% CO in air.

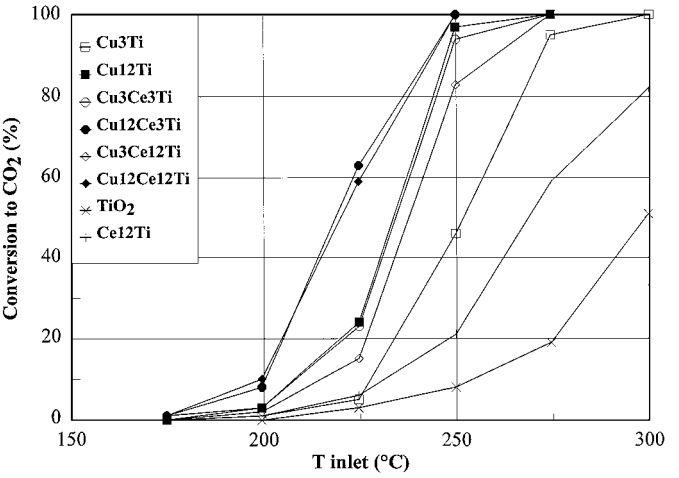

FIG. 4. Comparison of CuO_x/TiO_2 and CuO_x-CeO_x/TiO_2 catalysts with different loadings of CuO_x and CeO_x, respectively, for the combustion of 400 ppm ethyl acetate in air.

over the prepared CuO_x/TiO_2 and CuO_x-CeO_x/TiO_2 catalysts as well as over the TiO_2 and Ce12Ti materials.

It is apparent that the activity increases with the loading of CuO_x; e.g., Cu12Ti is considerably more active than Cu3Ti and requires 25–40°C lower inlet temperature to give the same conversion level. Addition of 3 μmol Ce/m^2 to the catalyst support produces enhanced activity, but there is no further improvement when the ceria loading is increased up to 12 μmol/m^2 surface area of the TiO_2 support. The two most active preparations are Cu12Ce3Ti and Cu12Ce12Ti, which have similar activity. The figure also shows that the CO oxidation activity, compared with the samples with copper, is negligible over TiO_2 and Ce12Ti.

In general, the differences between the catalysts concerning the inlet temperature which is required for giving a certain conversion becomes smaller at conversions over 90%. This is due to increased influence from mass transfer limitations at high conversions (20).

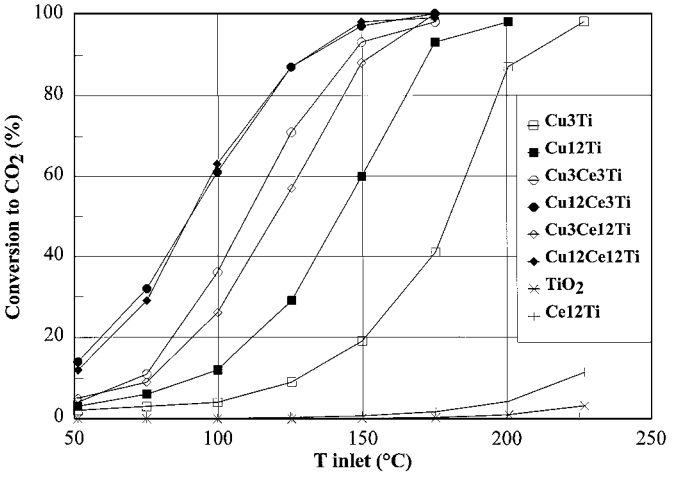

FIG. 3. Comparison of CuO_x/TiO_2 and CuO_x-CeO_x/TiO_2 catalysts with different loadings of CuO_x and CeO_x, respectively, for the oxidation of 0.2 vol% CO in air.

Complete oxidation of 400 ppm ethyl acetate in air. Figure 4 shows the results for the oxidation of 400 ppm ethyl acetate in air to CO_2 and H_2O over the prepared CuO_x/TiO_2 and CuO_x-CeO_x/TiO_2 catalysts, and the TiO_2 and Ce12Ti support materials. Similar trends as is seen in Fig. 3 for the oxidation of CO can here be observed; however, with the exception that the Cu12Ti catalyst is slightly more active than the Cu3Ce3Ti and Cu3Ce12Ti catalysts and that the TiO_2 and Ce12Ti support materials show a relatively higher activity to CO_2. Nevertheless the activities of all the copper catalysts are substantially higher. Figure 4 shows that the activity increases with the increase in the CuO_x loading. Compared with the Cu12Ti catalyst, the inlet temperature to the Cu3Ti catalyst has to be about 15–25°C higher to give the same conversion. The addition of CeO_x increases the activity relatively to the Cu12Ti catalyst. However, an amount in excess of 3 μmol Ce/m^2 surface area of the support has no influence, and the two most active catalysts are Cu12Ce12Ti and Cu12Ce3Ti, which both give complete combustion of ethyl acetate at 250°C.

Even though Fig. 4 shows the conversion of ethyl acetate to CO_2, which is the end product in catalytic waste gas incineration, it is also important to know if any by-products are formed and if any of these are more harmful than the reactant. Figure 5 shows the yield of CO_2, ethanol, acetaldehyde, and acetic acid during ethyl acetate oxidation in dry air over Cu12Ce12Ti (Fig. 5A), which is one of the best catalysts containing CeO_x, and Cu12Ti (Fig. 5C), which is the best catalyst without CeO_x. From the figures it is obvious that all ethyl acetate is not oxidised directly to CO_2 and H_2O. Over both catalysts ethanol and acetaldehyde are

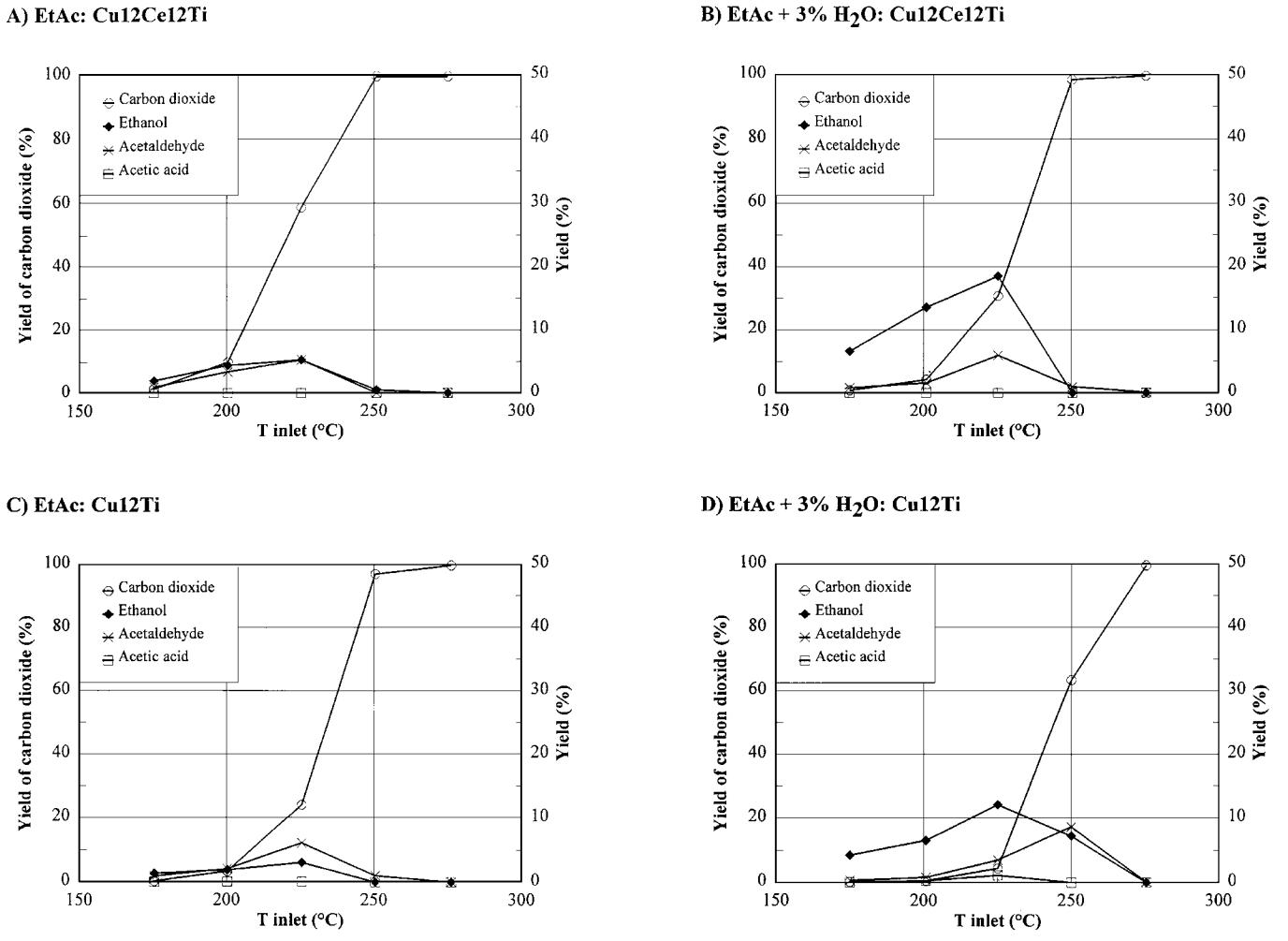

FIG. 5. Yield of ethanol, acetaldehyde, acetic acid, and carbon dioxide during the oxidation of 400 ppm ethyl acetate in dry and humid (3 vol% H_2O) feeds over a CuO_x/TiO_2 and a CuO_x-CeO_x/TiO_2 catalyst. The yield of carbon dioxide (left axis) and the yield of ethanol, acetaldehyde and acetic acid (right axis) for (A) Cu12Ce12Ti, dry feed; (B) Cu12Ce12Ti, humid feed; (C) Cu12Ti, dry feed; and (D) Cu12Ti, humid feed.

formed as intermediates. The yields of acetaldehyde and ethanol are of similar magnitude over both catalysts and pass through maxima of ~6% at around 225°C.

Experiments were also performed with water vapour in the feed, since in applications water is usually present in the waste gas. Figures 5B and 5D show the yield of CO_2, ethanol, acetaldehyde, and acetic acid during oxidation of ethyl acetate in the presence of 3 vol% water vapour over Cu12Ce12Ti and Cu12Ti, respectively. The activity of both the catalysts is slightly decreased when water vapour is added to the feed. For Cu12Ce12Ti (cf. Figs. 5A and 5B) the yield of ethanol is substantially increased when the feed contains water and has a maximum of 18% at 225°C, while the yield of acetaldehyde is only slightly affected by the presence of water. The results for Cu12Ti (cf. Figs. 5C and 5D) show similar behaviour and also the formation of a small amount of acetic acid. When water vapour is fed the maximum yield of ethanol over Cu12Ti is around 12% and appears at 225°C and the maximum yield of acetaldehyde is around 8% at 250°C. For acetic acid formation there is a 1% maximum at 225°C.

Complete oxidation of 800 ppm ethanol in air. The Cu12Ce12Ti and Cu12Ti catalysts were also tested for the oxidation of ethanol. Figures 6A and 6C show the yield of CO_2, ethyl acetate, acetaldehyde, and acetic acid over Cu12Ce12Ti and Cu12Ti, respectively. Compared with Cu12Ce12Ti, the activity of Cu12Ti is slightly less and the inlet temperature to the catalyst has to be 15°C higher to give the same conversion level. Over both catalysts the yield of acetaldehyde passes through a maximum of about 30% at 200°C, and also a small amount of ethyl acetate is formed around 200°C. Comparison of Figs. 6A and 6B, showing data for Cu12Ce12Ti without and with water vapour in the feed, respectively, reveals that the activity for the combustion of ethanol is less when there is 3 vol% water in the feed.

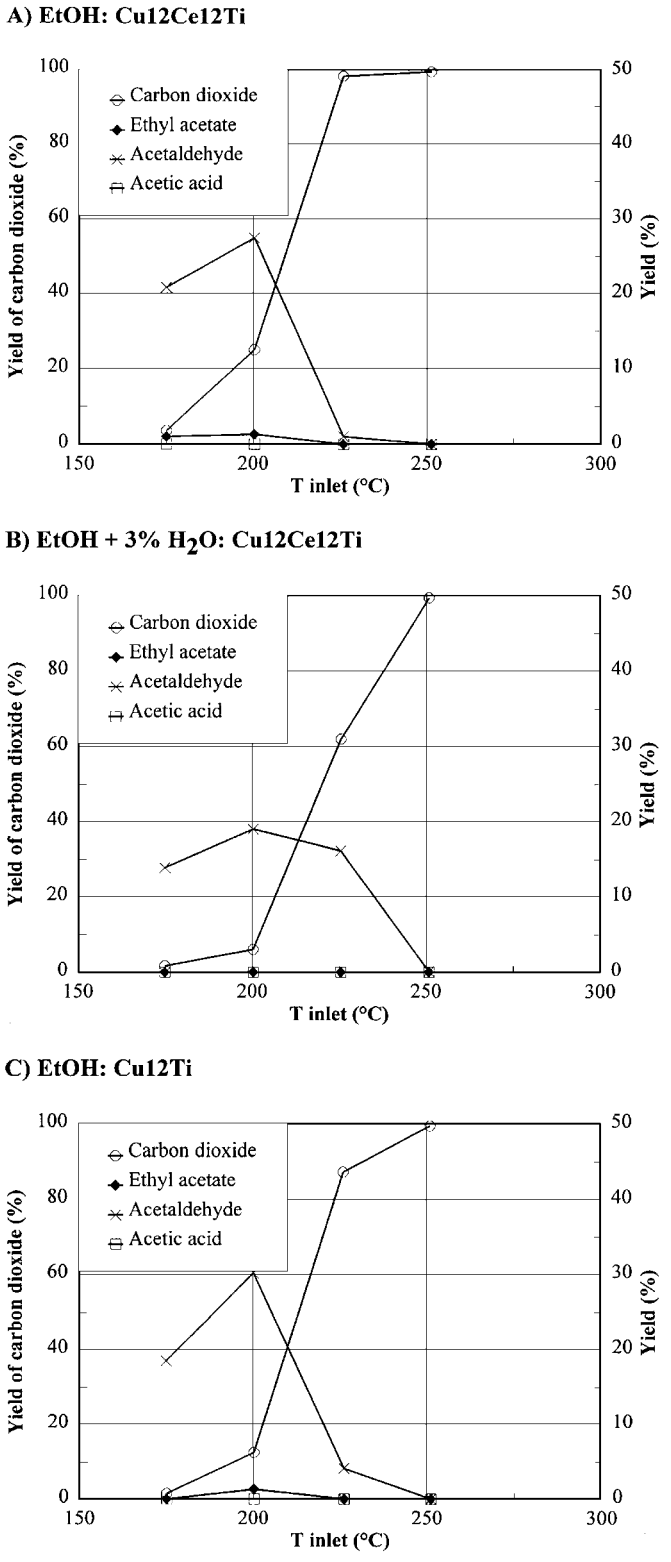

FIG. 6. Yield of ethyl acetate, acetaldehyde, acetic acid, and carbon dioxide during the oxidation of 800 ppm ethanol in dry and humid (3 vol% H_2O) feeds over a CuO_x/TiO_2 and a CuO_x-CeO_x/TiO_2 catalyst. The yield of carbon dioxide (left axis) and the yield of ethyl acetate, acetaldehyde, and acetic acid (right axis) for (A) Cu12Ce12Ti, dry feed; (B) Cu12Ce12Ti, humid feed; and (C) Cu12Ti, dry feed.

However, the yield of acetaldehyde is still high and is 19% at 200°C and, moreover, at 225°C the yield of acetaldehyde is considerably higher as compared to feeding no water. For both types of feed complete conversion of ethanol to CO_2 is obtained at 250°C.

Complete oxidation of a mixture of ethyl acetate and ethanol in the presence of water. The Cu12Ce12Ti catalyst was tested in the oxidation of a mixture containing 230 ppm ethyl acetate, 430 ppm ethanol, and 3 vol% H_2O in air. Due to partial oxidation of a small amount of the ethanol in the preheater and the stainless steel pipes, the inlet gas to the reactor also contained about 15 ppm acetaldehyde. Figure 7 shows the inlet concentration and the product distribution after the catalyst at different inlet catalyst temperatures, together with the conversion to CO_2. The figure shows that as the ethyl acetate concentration decreases, the ethanol concentration in the outlet increases up to 200°C. Simultaneously, some of the ethanol is partially oxidised to give acetaldehyde, the concentration of which passes through a maximum at 225°C. Above 200°C the formation of CO_2 starts to increase, but acetaldehyde and ethanol are still detected up to 250°C. Complete conversion to CO_2 is achieved at 275°C.

Specific Surface Area, Pore Size Distribution, and Pore Volume

Table 1 shows specific surface area, pore size distribution, and pore volume of the different samples. In general the BET surface area and the pore volume both decrease slightly, and the pore size distribution does not change with increased loading of cerium and copper. The decrease in surface area is still observed, although less pronounced, if the surface area is expressed in m^2/g of the support instead of m^2/g of the catalyst. Compared with the materials with cerium, the BET surface area is much less and the average pore size is larger for the Cu12Ti catalyst. This difference is due to the stabilising effect caused by the cerium.

X-Ray Diffraction

X-ray diffraction shows the presence of TiO_2 anatase (JCPDS file no. 21-1272) (19) in all samples. For the samples with 12 μmol CeO_x/m^2 (see Table 2) the XRD patterns show a very weak peak around 14.2–14.3°Θ, which corresponds to the strongest line (111) from CeO_2 (JCPDS file no. 34-394) (19). No peaks were observed from CuO, which should give strong reflections at 17.8°Θ and 19.4°Θ (JCPDS file no. 41-254) (19). Although interference is possible between the (200) line from CuO at 19.4°Θ and the (112) anatase line at 19.2°Θ, the intensity of this region was the same irrespective of CuO_x being present or not in the sample.

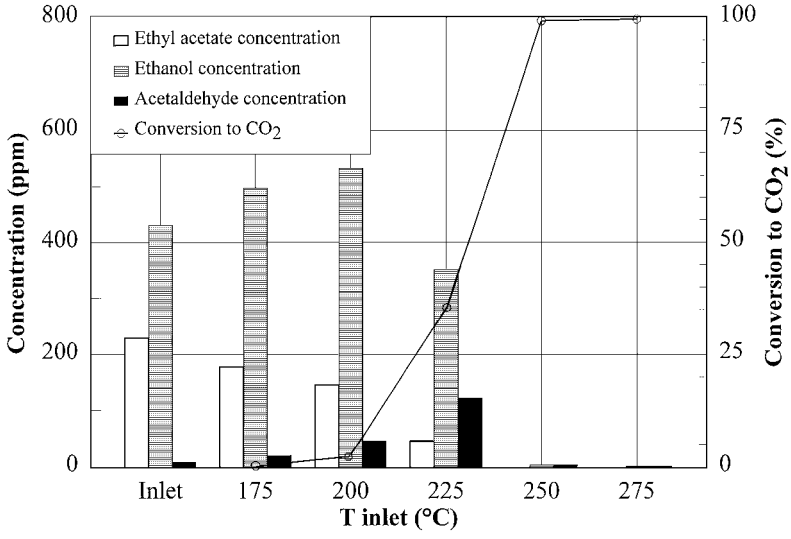

FIG. 7. Oxidation of a mixture containing 230 ppm ethyl acetate, 430 ppm ethanol, and 3 vol% water in air over the Cu12Ce12Ti catalyst. Outlet concentrations of detected hydrocarbons (left axis) are given for different inlet temperatures. The corresponding inlet concentrations as measured after the preheater (inlet) are also shown. The line plot shows the conversion to CO_2 (right axis).

Temperature-Programmed Reduction

CeO_x on TiO_2. Figure 8 shows the TPR-profiles for the pure TiO_2 support and the TiO_2 support loaded with 3 and 12 μmol CeO_x/m^2. The pure TiO_2 support has a reduction peak with maximum at 643°C. With increasing amount of CeO_x this peak shifts towards lower temperature. For Ce3Ti the peak maximum is at 602°C and for Ce12Ti at 581°C. Simultaneously as the peak shifts towards lower temperature, it increases in size. The peak area for Ce3Ti and Ce12Ti is 23% and 54% larger, respectively, compared with that for the pure TiO_2. A small broad peak with maximum around 725°C also appears for Ce12Ti.

CuO_x on TiO_2. Figure 9 shows the TPR-profiles for the pure TiO_2 support and the TiO_2 support loaded with 3 and 12 μmol CuO_x/m^2. The reduction peak for the pure TiO_2 with a maximum at 643°C shifts towards lower temperature with addition of CuO_x, because copper catalyses the reduction of TiO_2 (13). The corresponding peak maximum appears at 395°C for the Cu3Ti catalyst and at 386°C for the Cu12Ti catalyst. The reduction profile of Cu3Ti shows additional peaks at 205, 214, and 242°C, while Cu12Ti shows maxima at 195 and 248°C, as well as a shoulder at 280°C. The TPR curve of pure CuO showed reduction in a single peak with a maximum at 340°C.

CuO_x on CeO_x/TiO_2. Figure 10 shows the TPR-profiles for 3 and 12 μmol CuO_x/m^2 loaded on Ce3Ti. The TPR-profile of Cu3Ce3Ti has a peak at 195°C, a shoulder at 235°C and a small peak at 290°C in addition to the typical reduction peak for TiO_2 at 434°C. The TPR-profile for Cu12Ce3Ti shows the first reduction peak maximum at

TABLE 2

Characteristic X-Ray Diffraction Peaks for the Different Samples

	Anatase (101)		CeO_2 (111)	
Sample	Θ (°)	FWHM[a] (°)	Θ (°)	$I/I_O \cdot 100$[b]
TiO_2	12.69	0.14		
Cu3Ti	12.69	0.14		
Cu12Ti	12.69	0.12		
Ce3Ti	12.70	0.14		
Cu3Ce3Ti	12.71	0.14		
Cu12Ce3Ti	12.71	0.14		
Ce12Ti	12.67	0.14	14.22	7
Cu3Ce12Ti	12.69	0.15	14.33	8
Cu12Ce12Ti	12.68	0.14	14.28	5

[a] Full width at half maximum.

[b] I/I_O: Ratio of the CeO_2 (111) peak intensity to that for the (101) anatase line.

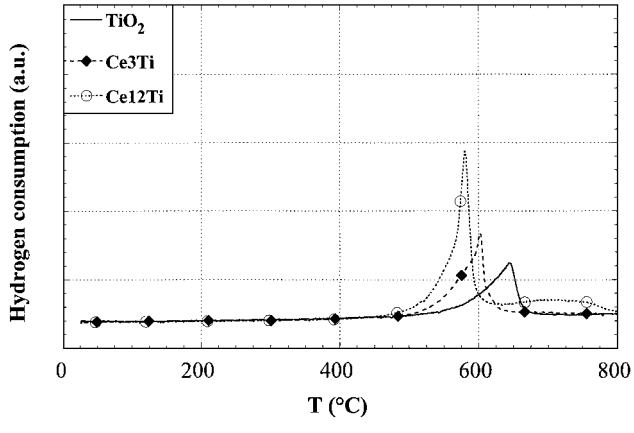

FIG. 8. TPR profiles for TiO_2, Ce3Ti, and Ce12Ti.

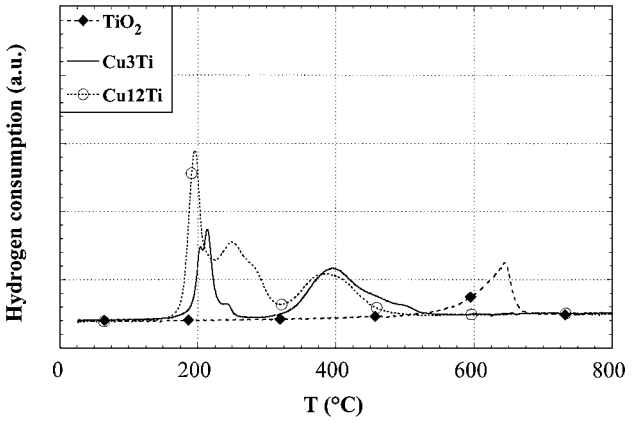

FIG. 9. TPR profiles for TiO_2, Cu3Ti, and Cu12Ti.

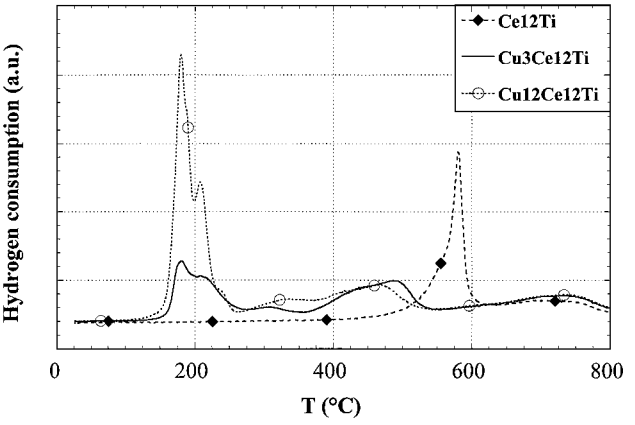

FIG. 11. TPR profiles for Ce12Ti, Cu3Ce12Ti, and Cu12Ce12Ti.

182°C (doublet). Additionally three small shoulders/peaks can be seen at 212, 245, and 286°C, and the typical peak due to reduction of TiO_2 is at 420°C.

Figure 11 shows the TPR-profiles for the loadings 3 and 12 μmol CuO_x/m^2 on the Ce12Ti support. The reduction profile of Cu3Ce12Ti shows a peak at 180°C and a shoulder at 208°C. Moreover, weak peaks appear at 306, 488, and 733°C. The Cu12Ce12Ti catalyst has the first reduction peak at 180°C with a shoulder at 185°C. Other peaks appear at 209, 335, 467, and 733°C.

FT-Raman Spectroscopy

CeO_x on TiO_2. Figure 12 shows the Raman spectra for TiO_2, CeO_2, and TiO_2 loaded with 3 and 12 μmol CeO_x/m^2 TiO_2. In Fig. 12A the four typical bands of TiO_2 anatase (21) at 143, 395, 516, and 639 cm^{-1} can be seen for all the samples containing TiO_2. For CeO_2 the typical strong band at 466 cm^{-1} (22) can be observed. Figure 12A clearly demonstrates that the intensity of the four typical bands of TiO_2 does not decrease when CeO_x has been loaded. Figure 12B shows that with a loading of 12 μmol CeO_x/m^2 (Ce12Ti) a band appears at 466 cm^{-1}, which corresponds to the strongest band of CeO_2. This band is not visible with a loading of 3 μmol CeO_x/m^2 TiO_2 (Ce3Ti).

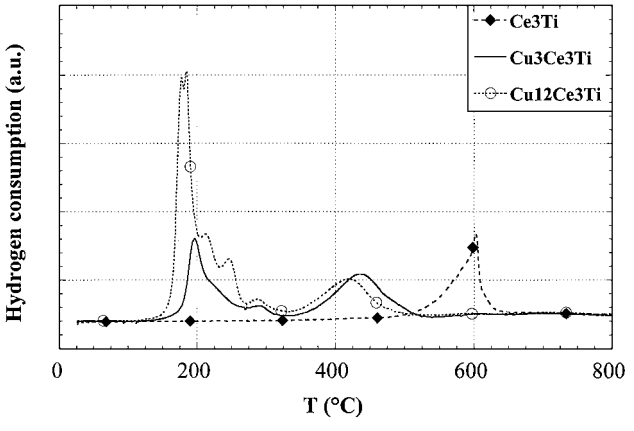

FIG. 10. TPR profiles for Ce3Ti, Cu3Ce3Ti, and Cu12Ce3Ti.

CuO_x on TiO_2. Figure 13A shows the Raman spectra when 3 and 12 μmol Cu/m^2 have been loaded on the TiO_2 support. It is evident that the intensities of the four typical TiO_2 bands decrease dramatically upon loading with copper. Compared with the pure support, the intensity of the strongest TiO_2 band at 143 cm^{-1} is 93% smaller for the Cu3Ti catalyst and 97% less for the Cu12Ti catalyst. In Fig. 13B a very weak band appears at 295 cm^{-1} for the Cu12Ti catalyst, which agrees with the position of the strongest band from CuO (23).

CuO_x on CeO_x/TiO_2. Figure 14A shows the Raman spectra after 3 and 12 μmol CuO_x/m^2 have been loaded on Ce3Ti and Ce12Ti. It is evident, just as is the case for the CuO_x/TiO_2 samples, that the intensities of the TiO_2 bands have decreased after deposition with CuO_x. In Fig. 14B it can be seen that the strongest band from CuO at 295 cm^{-1} appears as a weak feature in the Raman spectra of Cu12Ce3Ti and Cu12Ce12Ti. The strongest band of CeO_2 at 466 cm^{-1} can be observed even after the Ce12Ti support has been loaded with 3 and 12 μmol CuO_x/m^2 (Cu3Ce12Ti and Cu12Ce12Ti, respectively). Moreover, the CeO_2 band at 466 cm^{-1} is weaker in the Raman spectrum of Cu12Ce12Ti than in the spectrum of Cu3Ce12Ti.

X-Ray Photoelectron Spectroscopy

Binding energies of some characteristic peaks and the Ce/Ti, Cu/Ti, Cu/Ce, and Cu/(Ce + Ti) surface ratios are given in Table 3, together with the ratio between the Cu $2p_{3/2}$ shake-up satellite and the main peak, and the contribution of the Ce $3d_{3/2}$ u‴ peak to the entire Ce 3d spectral region. The notations used by other investigators (22, 24–26) for the peaks in the Ce 3d region have been adopted and are shown in Fig. 15A.

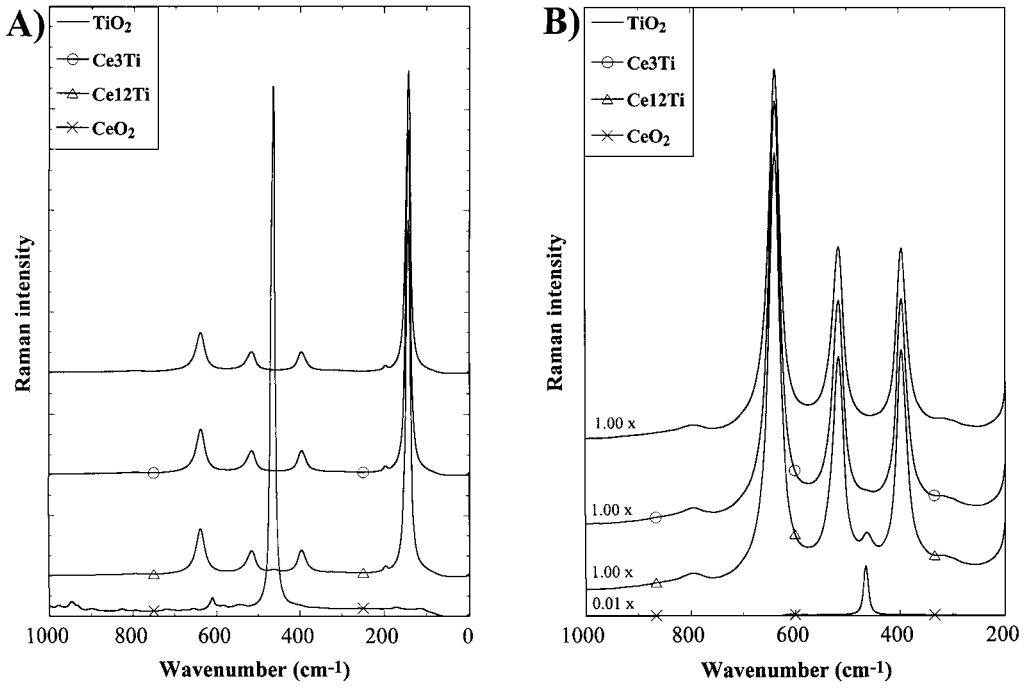

FIG. 12. Raman spectra of TiO_2, CeO_2, and CeO_x/TiO_2 in (A) the region 0–1000 cm^{-1}; and (B) the region 200–1000 cm^{-1} with factors inserted by which the Raman intensity has been multiplied.

The Cu $2p_{3/2}$ binding energy (Table 3 and Fig. 15B) is 934.2 eV for the pure CuO and in the range 934.2–934.6 eV for copper on the supports, except for Cu3Ti showing a slightly lower value, 933.6 eV. The intensity ratio between the Cu $2p_{3/2}$ shake-up satellite at ∼944 eV and the main peak is 0.52 for the pure CuO and in the range 0.42–0.52 for the supported copper, with the exception that the ratio is 0.34 for Cu3Ti. The lower ratios for the supported copper, and

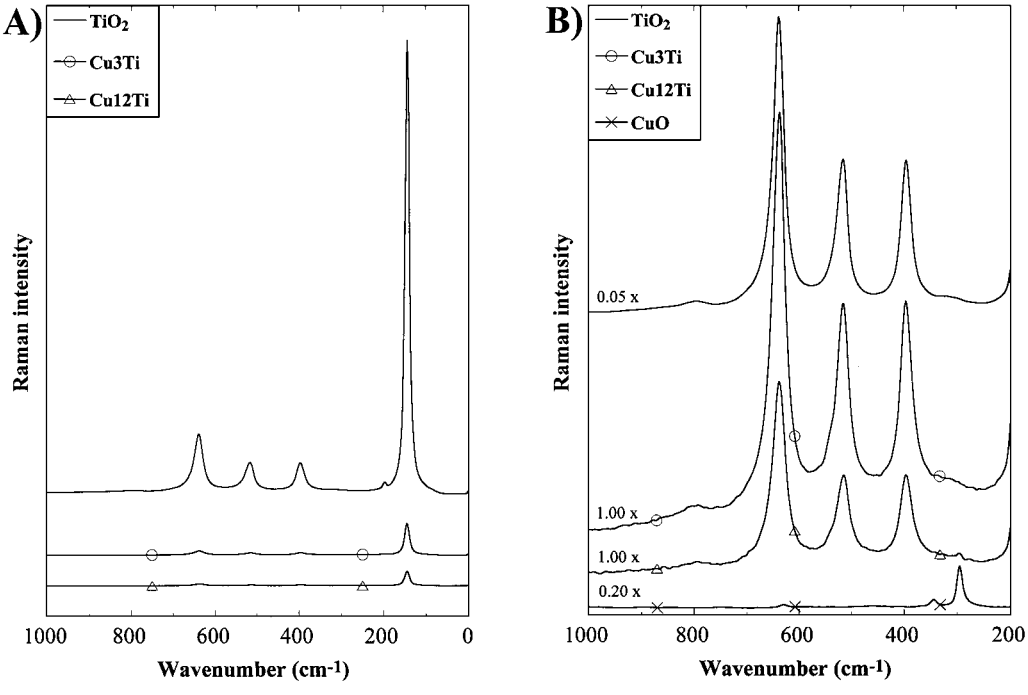

FIG. 13. Raman spectra of TiO_2, CuO, and CuO_x/TiO_2 in (A) the region 0–1000 cm^{-1}; and (B) the region 200–1000 cm^{-1} with factors inserted by which the Raman intensity has been multiplied.

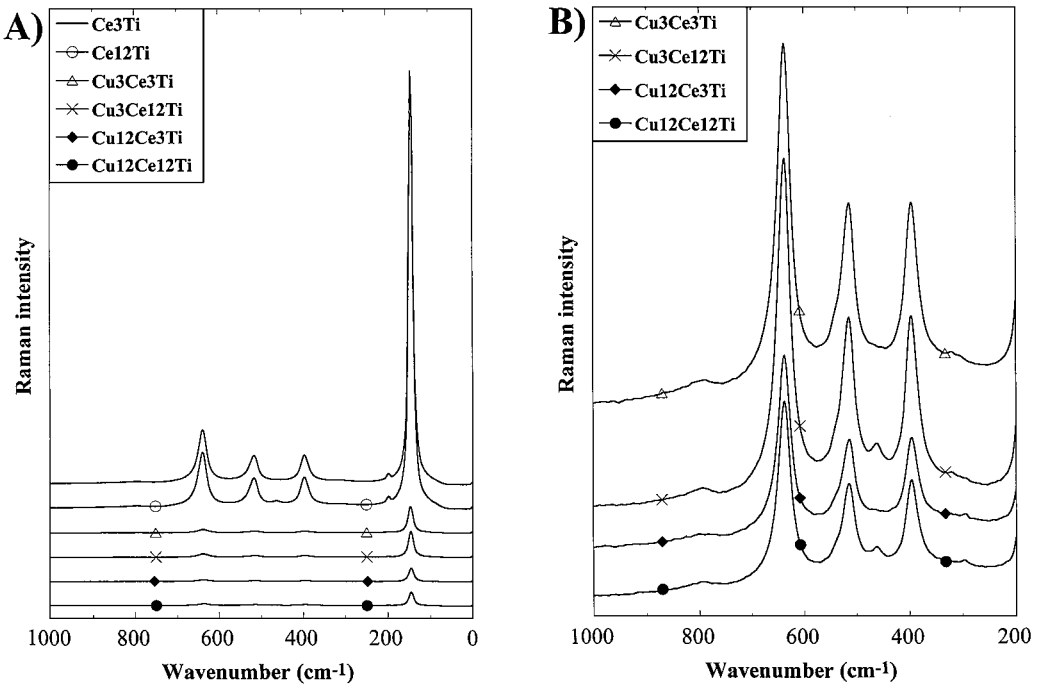

FIG. 14. Raman spectra for CeO_x/TiO_2 and CuO_x-CeO_x/TiO_2 in (A) the region 0–1000 cm^{-1}; and (B) the region 200–1000 cm^{-1}.

especially for Cu3Ti, are most likely due to photoreduction of the dispersed copper in the spectrometer. For the copper catalysts it was observed that increase of the analysis time causes a decrease of the ratio and a shift of the Cu $2p_{3/2}$ binding energy to about 932.7 eV. This behaviour shows that reduction of Cu^{2+} to Cu^{1+} occurs in the spectrometer, in agreement with a corresponding shift in the kinetic energy of the Cu $L_{2,3}M_{4,5}M_{4,5}$ Auger line (27). However, it was impossible to use very short analysis times, because in this case the signal to baseline ratio was too low.

The Ti $2p_{3/2}$ binding energies in Table 3 are close to 458.7 eV for all samples and agree with the published data for TiO_2 (28). The Cu/Ti, Cu/Ce, and Cu/(Ce + Ti) atomic ratios increase with the increase in copper loading. For the

TABLE 3

XPS Data Measured for the Different Samples

Sample	Cu $2p_{3/2}$[b] BE[a] (eV)	Ce3d[c] BE[a] (eV) u‴[e]	Ce3d[c] BE[a] (eV) v[e]	Ti $2p_{3/2}$[b] BE[a] (eV)	Atomic ratio[c] Ce/Ti	Atomic ratio[b] Cu/Ti	Atomic ratio[d] Cu/Ce	Atomic ratio[d] Cu/(Ce + Ti)	Ce[c] u‴[e]/Ce 3d	Cu $2p_{3/2}$ ratio[b] satellite/main peak
TiO_2	—	-	-	458.8	-	-	-	-	-	-
CuO	934.2	-	-	-	-	-	-	-	-	0.52
CeO_2	-	916.8	882.6	-	-	-	-	-	0.11	-
Cu3Ti	933.6	-	-	458.8	-	0.10	-	0.08	-	0.34
Cu12Ti	934.2	-	-	458.6	-	0.23	-	0.18	-	0.42
Ce3Ti	-	916.5	882.5	458.7	0.10	-	-	-	0.04	-
Cu3Ce3Ti	934.3	917.0	882.9	458.6	0.06	0.12	1.5	0.08	0.05	0.47
Cu12Ce3Ti	934.6	916.8	882.7	458.6	0.04	0.21	5.0	0.18	0.05	0.52
Ce12Ti	-	916.5	882.4	458.8	0.19	-	-	-	0.10	-
Cu3Ce12Ti	934.2	916.9	882.7	458.7	0.13	0.10	0.8	0.08	0.11	0.44
Cu12Ce12Ti	934.6	917.0	882.9	458.6	0.12	0.22	1.8	0.16	0.11	0.47

[a] Binding energy.
[b] Analysed with the Mg anode.
[c] Analysed with the Al anode.
[d] Atomic ratio analysed with the Al anode and the Cu $2p_{5/2}$ shake-up satellite area excluded.
[e] Peaks denoted according to Fig. 15A.

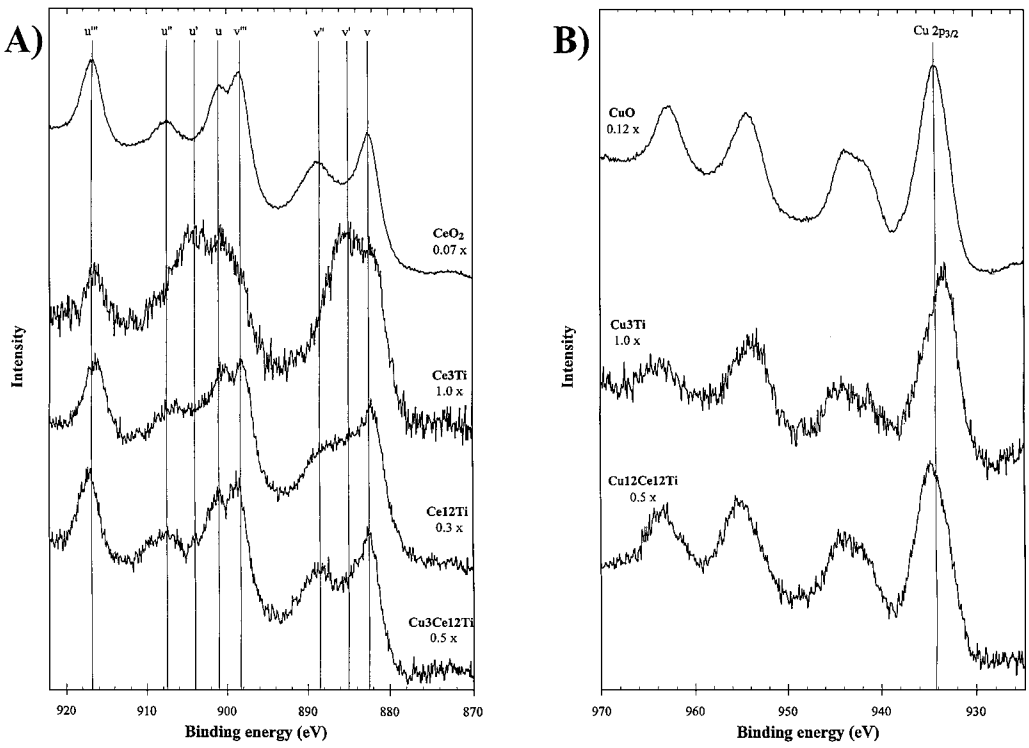

FIG. 15. XPS spectra of (A) the Ce 3d region as measured with an Al-anode for the CeO_2, Ce3Ti, Ce12Ti, and Cu3Ce12Ti samples; and (B) the Cu 2p region as measured with a Mg-anode for the CuO, Cu3Ti, and Cu12Ce12Ti samples. Factors by which the intensity has been multiplied are inserted.

CeO_x/TiO_2 samples an increase in the Ce/Ti ratio is observed with increase in the cerium content. The ratio, however, is lower for the corresponding samples with copper.

Ce 3d core level spectra are shown in Fig. 15A for CeO_2, Ce3Ti, Ce12Ti, and Cu3Ce12Ti. The series of peaks denoted by v and u are from the $3d_{5/2}$ and $3d_{3/2}$ states, respectively. The v and v″ peaks have been assigned to a mixing of $3d^94f^2(O\ 2p^4)$ and $3d^94f^1(O\ 2p^5)$ Ce(IV) final states, and v‴ to the $3d^94f^0(O\ 2p^6)$ Ce(IV) final state. The peak indicated v′ is from the $3d^94f^1(O\ 2p^6)$ Ce(III) final state (26). The series of u structures from the $3d_{3/2}$ level can be explained in the same way. Considering Table 3, the binding energies of the u‴ and v peaks for the pure CeO_2 are 916.8 and 882.6 eV, respectively, and no v′ and u′ features are apparent in the CeO_2 3d spectrum (Fig. 15A). For the cerium supported on titania, the binding energy for the u‴ peak is around 916.5–917.0 eV and for the v peak it is about 882.5–882.9 eV.

For the samples with cerium the ratio between the intensity of the u‴ peak to the total intensity of the Ce 3d region is included in Table 3. The ratio is 0.11 for the pure CeO_2, and the value is similar for the samples with the highest content of cerium (Ce12Ti, Cu3Ce12Ti, and Cu12Ce12Ti). For the samples with the lower cerium content (Ce3Ti, Cu3Ce3Ti, and Cu12Ce3Ti), however, the ratio is only half. According to Shyu *et al.* (22), the fraction of the u‴ peak to the total Ce 3d intensity depends on the Ce^{4+}/Ce^{3+} ratio. Reduction of Ce^{4+} causes an increase of the v′ and u′ peaks from Ce^{3+} states (24–26). Considering that u′ and v′ peaks are clearly present in the Ce 3d spectrum for Ce3Ti in Fig. 15A and that the u‴/Ce 3d region ratio in Table 3 for this sample is lower than the ratio for CeO_2, it follows that a fraction of the cerium in the Ce-doped support is present as Ce^{3+}. This fraction does not seem to be changed by the deposition of copper. Likewise for dispersed copper, however, one has to be aware of the possibility to have photoreduction of dispersed cerium in the spectrometer (29). For the samples containing ceria dispersed on titania, with increased analysis time we could observe a decrease in the area ratio between the u‴ peak to the total Ce 3d region, simultaneously as the v′ and u′ peaks increased in size. This behaviour shows that reduction of Ce^{4+} to Ce^{3+} occurs in the spectrometer. For example, the u‴/Ce 3d area ratio decreased by about 35% during 45 min for the Ce12Ti sample, and the main part of the reduction occurred during the first 30 min.

DISCUSSION

Stabilisation of Titania in the Presence of Copper

In our previous reports (13, 30) we have shown that CuO_x on TiO_2 (anatase), compared with other combinations of active metal oxides and supports, gives good activity for the combustion of VOCs. However, we observed deactivation of the catalyst during use in the incinerator of a formaldehyde plant. Typically, a CuO_x/TiO_2 catalyst with

12 μmol Cu/m^2 loses 38% of the surface area during two months in operation. Characterisation showed sintering of both the support and the active phase (13). The results in Fig. 1 show that unstabilised CuO_x/TiO_2, compared with the pure support, sinters considerably during heat treatment. Obviously, the presence of copper induces sintering of the titania, which also has been observed by other investigators (15, 31, 32). Comparison of the results in Fig. 1 shows upon the possibility to obtain stabilisation using additives with Al, Ce, K, and La. Stabilisation of anatase with alumina (14) and potassium (15, 33) has previously been reported in the literature. In the present case samples with cerium were selected for more detailed investigation, considering that cerium not only stabilises the titania but, unlike the other additives investigated (Fig. 2), it also enhances the catalytic activity of the CuO_x on titania. The observation that cerium retards sintering and crystallite growth of TiO_2 covered with copper agrees with the FWHM value of the (101) anatase line in Table 2 being smaller for Cu12Ti than for the samples containing cerium. In our previous work (13), we observed a direct relationship between the FWHM value for anatase and the specific surface area. Consequently, the observed sintering of anatase in the presence of copper is real and not apparent.

Stabilisation of a material towards sintering generally can be achieved by (i) change of the chemical composition by doping of the bulk or the surface and (ii) addition of a textural promoter, preventing contact between crystallites. The first option usually will change also the catalytic property of the material. For the CuO_x/TiO_2 catalysts stabilised with cerium, the second option that CeO_2 acts as a textural promoter can be excluded to explain the stabilising effect. Enough number of small crystallites of CeO_2, preventing the TiO_2 crystals from being in contact with either each other or copper, can hardly form at the low cerium content that here is used in the preparations. Instead, either decoration of the titania surface with Ce species, or dissolution of Ce ions in the titania can explain the stabilisation effect seen in Fig. 1. Considering the considerable difference between the crystal radii of cerium and titanium ions (34), e.g. 0.68 and 1.01 Å for Ti^{4+} and Ce^{4+}, respectively, it is unlikely for cerium ions to dissolve into the bulk of TiO_2. Moreover, no formation of $CeTiO_3$ (35) was observed, which agrees with that the formation of this phase with Ce^{3+} and Ti^{3+} ions requires reducing conditions. The observation using XRD (Table 2) and Raman spectroscopy (Fig. 12) that CeO_2 is not formed before the cerium content is increased from 3 (Ce3Ti) to 12 (Ce12Ti) μmol Ce/m^2 surface area of the support indicates that a limited amount of cerium can be confined to the titania surface. Additional support for this inference is found considering the XPS data for Ce3Ti and Ce12Ti in Table 3, showing efficient spreading of cerium on the titania surface. The Ce/Ti atomic ratio is 0.10 and 0.19 for Ce3Ti and Ce12Ti, respectively. Assuming that all Ce ions in Ce3Ti are at the surface and considering that the ratio increases almost a factor two when the cerium content is increased by a factor of 4, the limit for the surface concentration can roughly be estimated to 6 μmol Ce/m^2. This value corresponds to approximately half of the cations at the surface. A surface layer with both cerium and titanium ions interacting possibly can form on the titania as a consequence of the surface being able to relax. The TPR profiles in Fig. 8 is in support of that a Ce-O-Ti surface structure exists. The pure titania gives a reduction peak at 643°C, which corresponds to removal of 2% of the oxygen in TiO_2. This value infers that the peak is related to reduction of the surface layer only. When the titania is stabilised with increasing amount of cerium, the corresponding peak both shifts towards lower temperature and increases in size. Peaks from the reduction of CeO_2 are observed only in the profile of Ce12Ti and appear as a very weak shoulder at ~515°C, which is almost invisible, and as a broad peak at 725°C. Comparing the TPR profiles of ceria samples with different surface area, Yao and Yao (36) obtained a similar reduction profile for CeO_2 and concluded that the former peak can been assigned to the reduction of the ceria surface and that the latter peak is due to reduction of the bulk. Obviously, the profiles in Fig. 8 show that the reducibility of the Ce-O-Ti surface in hydrogen is more difficult than that of CeO_2 but easier than that of TiO_2.

As described under Results, we observed that some reduction of Ce^{4+} to form Ce^{3+} species occurs in the X-ray photoelectron spectrometer. Therefore, the valence of the cerium which is confined to the support surface cannot fully be determined. However, the u‴/Ce 3d ratios in Table 3 for Ce3Ti, both without and with copper, indicate that at least a part of the dispersed cerium is Ce^{3+} (22). This proposal agrees with the XPS spectrum of Ce3Ti in Fig. 15A showing u′ and v′ features, which are typical for Ce^{3+} species (24–26).

Structure of CuO_x on TiO_2

In our previous investigation of CuO_x/TiO_2 catalysts (13) we found that the activity for the combustion of CO and toluene increases with the copper loading up to 12 μmol Cu/m^2 surface area of the support, corresponding to a theoretical monolayer of CuO_x on titania. At higher loading crystalline CuO was formed, contributing little to the active surface area and, thus, the activity of the catalyst. The results in Figs. 3 and 4, showing that Cu12Ti is considerably more active than Cu3Ti for the combustion of CO and ethyl acetate, respectively, are in line with our previous finding and show efficient dispersion of copper on titania up to 12 μmol Cu/m^2 surface area. The Raman spectra in Fig. 13 confirm that dispersed copper oxide is formed on the titania. Compared with the spectrum of the pure support, it is observed that the Raman intensity of the titania bands is considerably less in the spectra for Cu3Ti and Cu12Ti. Only

a very weak peak at 295 cm^{-1} from bulk CuO (23) is apparent in the spectrum for Cu12Ti in Fig. 13B. However, no reflections from CuO were observed in the XRD patterns of Cu3Ti and Cu12Ti. The XPS data in Table 3 also agree with the dispersion of copper being good. The Cu/Ti surface ratio increases from 0.10 to 0.23 when the copper loading is increased from 3 (Cu3Ti) to 12 (Cu12Ti) μmol Cu/m^2. The appearance of some CuO in Cu12Ti obviously can be seen as a consequence of the copper induces sintering of the titania during the calcination (Table 1) and the loading for this sample, which corresponds to a monolayer of CuO on TiO_2, was calculated on the basis of the surface area of the fresh support.

For the interpretation of the TPR profiles of Cu3Ti and Cu12Ti in Fig. 9 it is of interest first to briefly summarise our earlier TPR results for CuO_x in various loading on TiO_2 (13). For a loading corresponding to 1/3 of a monolayer with CuO_x on TiO_2 (anatase) we observed a reduction peak at ∼200°C. For theoretical loadings in the range 1–5 monolayers of CuO_x the profiles showed a peak at ∼180°C, having a constant area which was independent of the loading. Another reduction peak appeared at higher temperature, which intensity increased with the increase in the loading concurrently as the peak maximum shifted from 230 to 280°C. Considering various characterisation results for freshly prepared and deactivated catalysts, the peak at ∼180°C was assigned to the polymeric copper species forming patches or a bidimensional layer, interacting with the titania surface. The peak at ∼200°C was assigned to the monomeric copper species interacting with the titania, and peaks in the region 230–280°C were identified as being due to the reduction of bulk CuO not interacting with the support. For all CuO_x/TiO_2 preparations there was an additional peak at ∼400°C, and the size of the peak was the same irrespective of the copper loading. It was proposed that this peak is due to reduction of the titania surface caused by the spillover of hydrogen from the copper metal which is formed at an earlier stage during the reduction process.

Considering the summary above, the TPR profiles in Fig. 9 for Cu3Ti and Cu12Ti can be interpreted as follows. The doublet peak around 210°C in the profile of Cu3Ti can be proposed to be from the monomeric copper species interacting with the support, and the peak at 195°C for Cu12Ti can be assigned to the polymeric copper species being attached to the titania. The somewhat higher temperature (∼10°C) for these two types of peaks, as compared to the temperatures that we reported in our previous work (13) reasonably are due to the different calcination temperature, a different titania preparation, and minor experimental differences. The small peak at 242°C in the profile of Cu3Ti and the peaks at 248 and 290°C which appear in the profile of Cu12Ti can all be assigned to CuO crystallites of various size (13, 37). For both reduction profiles the broad peak around 390°C can be due to copper-catalysed reduction of the titania surface (13), since the reduction peak which appears at 643°C for the pure support is absent in the profile of both Cu3Ti and Cu12Ti. The reduction profiles described show good agreement with those reported by Wöllner and co-workers (37) for CuO_x/TiO_2 preparations being calcined at a similar temperature. The interpretation that on titania there are both dispersed CuO_x species, interacting with the titania, and CuO crystallites agrees with the conclusions of other investigators which were based on TPR (38) and diffuse reflectance data (39).

To address the valence of the different types of dispersed copper species, the XPS results in Table 3 can be considered. The Cu $2p_{3/2}$ binding energies for Cu3Ti and Cu12Ti are 933.6 and 934.2 eV, respectively, and the corresponding value for CuO is 934.2 eV. For the Cu^{1+} species in Cu_2O the Cu $2p_{3/2}$ binding energy has been reported to be about 1.3 eV less than for Cu^{2+} in CuO (27). Another difference between Cu^{1+} and Cu^{2+} compounds is that the latter have a Cu $2p_{3/2}$ shake-up satellite peak at ∼944 eV and a satellite/main peak ratio in the range 0.3–0.9 (40), while Cu^{1+} compounds give no satellite. The ratio in Table 3 for CuO is 0.52 and for Cu3Ti and Cu12Ti the measured ratios are 0.34 and 0.42, respectively. Thus, the Cu $2p_{3/2}$ binding energy values and the satellite/main peak ratios in Table 3 suggest that the polymeric copper species in Cu12Ti contains Cu^{2+}, while some of the monomeric species on Cu3Ti are Cu^{1+}. However, in this regard it is important to be aware that dispersed copper species usually are more sensitive than bulk CuO to photoreduction in the spectrometer, which also was observed in the present investigation. Therefore, we cannot exclude that the monomeric species are divalent in an atmosphere with oxygen.

Structure of CuO_x on CeO_x-TiO_2

Comparison of the morphological data in Table 1 shows only small differences in specific surface area, pore volume, and pore size distribution between Ce3Ti, Ce12Ti, and their counterparts being covered with CuO_x. The XRD data in Table 2 shows the presence of bulk CeO_2 on neither Ce3Ti, nor Cu3Ce3Ti and Cu12Ce3Ti. CeO_2 is, however, present in small amounts on Ce12Ti, Cu3Ce12Ti, and Cu12Ce12Ti. None of the samples with copper showed diffraction lines from crystalline CuO. Comparison of the Raman spectra in Figs. 13 and 14 for CuO_x on TiO_2 and CeO_x/TiO_2, respectively, shows the dispersion of copper being of similar magnitude on both types of support. In both cases, the intensity of the bands from TiO_2 is considerably less after deposition with copper. As for Cu12Ti (Fig. 13B), a small peak from crystalline CuO is present in the Raman spectra for the CeO_x/TiO_2 samples with the highest copper loading, i.e. Cu12Ce3Ti and Cu12Ce12Ti (Fig. 14B). All these results give evidence for the dispersion of copper being good on cerium modified titania. The observation that the intensity of the Raman bands of titania strongly decreases upon

deposition with copper species (Figs. 13A and 14A) but not with cerium species (Fig. 12A), despite the dispersion of Cu and Ce being similar (Table 3), can be due to that the two types of species have different electron structure and therefore affect differently the scattering property of the material. It is a fact that the samples with copper are coloured which can induce heating effects influencing the Raman intensity (41). Likewise CuO_x, the deposition of vanadia on titania has been reported (42) to cause a dramatic decrease in the intensity of the Raman bands from TiO_2, which was observed both using Ar and Nd : YAG lasers.

Before considering the TPR profiles from the CuO_x-CeO_x/TiO_2 samples, it is worthy of note that the cerium content in the samples is low and that CeO_2 is present in small amount mainly in the samples with the Ce12Ti support. Even though CuO_x on CeO_2 gives a TPR peak below 200°C from a finely dispersed species (43), in the present case the contribution from bulk CeO_2 to the total surface area is negligible, and the number of surface atoms on the ceria is small as compared with the total number of copper atoms being deposited. Therefore, it is reasonable to discuss the TPR results mainly in terms of the copper species as being attached to the Ce-doped titania surface and to make comparisons with the profiles of Cu3Ti and Cu12Ti which were analysed in the previous section. The TPR profiles in Figs. 10 and 11 from the CuO_x-CeO_x/TiO_2 samples, compared with the profiles in Fig. 9 from Cu3Ti and Cu12Ti, generally show peaks from dispersed copper at slightly lower temperature. This shift in reduction temperature indicates interaction between copper and cerium and that the reduction of the copper species by hydrogen is promoted by the cerium. The TPR profile in Fig. 10 from Cu3Ce3Ti has a peak at 195°C from a dispersed copper species, possibly a monomeric species (13), interacting with the surface. In comparison with the profile of Cu3Ti in Fig. 9, it seems that the two peaks which in that case were assigned to monomeric species have merged together after doping with cerium. Moreover, the profile of Cu3Ce3Ti in Fig. 10 shows a broad shoulder starting at 210°C and a small peak at 290°C, both of which can be assigned to dispersed CuO particles not interacting with the Ce-doped support.

The TPR profile of Cu12Ce3Ti in Fig. 10 and the profile of Cu12Ce12Ti in Fig. 11 both show two peaks at 180 and 185°C, respectively. Considering the good dispersion of copper, together with the previous discussion on the TPR profiles of CuO_x/TiO_2, these two peaks can be assigned to polymeric copper species in form of patches or a bidimensional layer interacting with the support (13). The appearance of two peaks can likely be related to polymeric CuO_x species at surfaces with a different arrangement between Ce and Ti ions, since the corresponding profile for Cu12Ti in Fig. 9 shows only one peak. For Cu12Ce3Ti the two peaks are of similar size. However, for Cu12Ce12Ti the peak at 180°C is larger than that at 185°C (shoulder), indicating that the former is from a species being attached to a part of the support surface being richer in cerium. The series of peak maxima at 212, 245, and 286°C in the profile of Cu12Ce3Ti in Fig. 10 can be from bulk CuO of different particle size (13, 37), a proposal that agrees with there being a band from CuO in the Raman spectrum of this sample in Fig. 14B. In the profile for Cu12Ce12Ti in Fig. 11, compared with the profile of Cu12Ce3Ti in Fig. 10, the peak at ~210°C is larger, the peak at 245°C is just seen as a shoulder and there is no peak at 286°C. The differences indicate that the particles of free CuO diminish in size with increased content of cerium. The profile in Fig. 11 for Cu3Ce12Ti shows the same peaks as Cu12Ce12Ti in the region around 200°C, indicating the presence of dispersed copper in form of polymeric species. Compared with the profile for Cu3Ce3Ti in Fig. 10, it seems that when the ceria content is increased, there is a transformation of monomeric copper species into dimeric or polymeric species. EPR measurements on CuO/CeO_2 preparations have shown the presence of Cu^{2+} in both isolated and dimeric form in addition to CuO (44).

The Cu $2p_{3/2}$ binding energy values and the shake-up satellite/main peak ratios for the CuO_x-CeO_x/TiO_2 samples, which are given in Table 3, agree with copper being in the divalent state. That the dispersion of copper is good agrees with the increase in the Cu/Ti and the Cu/Ce atomic ratios when the copper content is increased. Comparison of the Ce/Ti ratios for Ce3Ti and Ce12Ti with those for Cu3Ce3Ti and Cu3Ce12Ti, respectively, shows that the ratio is less after the copper has been deposited. When the copper content is further increased as for Cu12Ce3Ti and Cu12Ce12Ti, there is almost no additional decrease in the ratio. This behaviour indicates that at low content the copper is preferentially bonded to the cerium atoms at the support, but when the loading with copper is increased then the distribution of copper between cerium and titanium sites becomes more even. Such a proposal agrees with the formation of mono and poly species of copper at a surface with the cerium being dispersed in the external layer of the titania.

Complete Oxidation over CuO_x/TiO_2 and CuO_x-CeO_x/TiO_2

The results in Figs. 3 and 4 for the combustion of CO and ethyl acetate, respectively, in air over the CuO_x/TiO_2 and CuO_x-CeO_x/TiO_2 catalysts show that the activity in both cases increases with the content of both copper and cerium. However, increased loading with CeO_x from 3 to 12 μmol/m^2 surface area of the support does not improve the performance for a fixed content of copper. This behaviour was demonstrated in a previous paragraph to be due to the limit for the dispersion of cerium at the titania surface and to formation of bulk CeO_2 at higher loading. Clearly, the addition of cerium increases the activity of the copper species. Our characterisation has shown that

dispersed copper species are formed up to a loading of about 12 μmol Cu/m^2 surface area of the support. This is in line with our previous work (13), where for higher copper loading we found that bulk CuO is formed, which contributes little to the surface area and activity of the catalyst. Figure 6 shows that the complete oxidation of ethanol over CuO_x/TiO_2 also is improved by the addition of cerium. Consequently, the activity for all the three reactions that have been studied in this work is improved by the addition of cerium to the catalyst. These results are in general agreement with those being reported by other investigators of CuO_x/CeO_2 catalysts. Liu and Flytzani-Stephanopoulos (45, 46) found that the Cu-Ce-O system is highly active for the combustion of both CO and methane. The same authors concluded that copper is finely dispersed on ceria at low copper content and that copper in excess forms CuO particles, contributing little to the activity. Similar results were obtained by Luo *et al.* (43), who found that the activity for CO oxidation increases up to a CuO loading of 3 wt% on CeO_2, corresponding to 7 μmol Cu/m^2. The TPR profiles in Figs. 9–11 indicate that there are two types of copper species interacting with the support, which were indicated as being monomeric and polymeric, respectively. Considering the results in Figs. 3 and 4 it is obvious that both species are active, but from the results it is impossible to conclude about which of the two species that is the most active per Cu atom. However, the TPR profiles suggest that the species being formed at low copper loading (monomeric) is the least active of the two, since its reduction peak appears at a higher temperature than that of the polymeric species. The Cu/(Ce + Ti) XPS ratio in Table 3 show no major influence from cerium on the dispersion of copper. Therefore the observation that the addition of cerium to the catalysts provides improved activity to the copper species can be explained, considering the TPR results. The TPR profiles, as were previously discussed, show upon interaction between cerium and copper facilitating by an electronic effect the reduction of the copper species.

Figure 6 shows considerable formation of acetaldehyde from ethanol before the conversion to carbon dioxide and water is complete. The reaction behaviour of Cu12Ti and Cu12Ce12Ti in this regard is similar, and the only difference is that Cu12Ti is somewhat less active than Cu12Ce12Ti. Addition of 3 vol% water to the feed to the Cu12Ce12Ti catalyst suppresses the activity, although it can be concluded that the addition does not change in general the reaction scheme. Considering that also ethyl acetate is detected in small amount, the results in Fig. 6 suggest that the combustion of ethanol occurs in the sequence ethanol → acetaldehyde → acetic acid → CO_2.

In the oxidation of ethyl acetate, both ethanol and acetaldehyde are formed over the Cu12Ti and Cu12Ce12Ti catalysts (see Fig. 5). With the addition of 3 vol% water to the feed, the activity is slightly decreased and especially the yield of ethanol is increased. This is probably due to the fact that the equilibrium (47)

$$CH_3COOH + C_2H_5OH \Leftrightarrow CH_3COOCH_2CH_3 + H_2O$$

shifts towards acetic acid and ethanol. The results in Fig. 5 indicate that the acetic acid formed is quickly oxidised to carbon dioxide and water. Actually, a few parts per million of acetic acid is detected over the Cu12Ti catalyst when using humid feed (Fig. 5D). Considering the results, a plausible mechanism can be as follows:

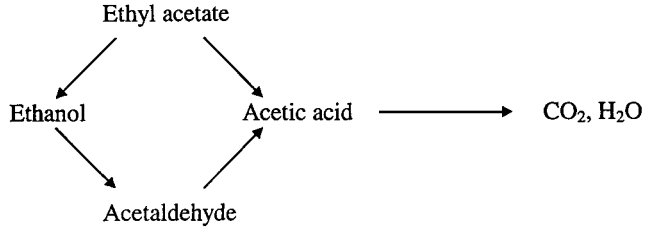

A waste gas stream with a mixture of ethyl, acetate, ethanol, and water in air is common in one segment of the printing industry. Figure 7 shows the result for the combustion of such a mixture over the Cu12Ce12Ti catalyst. The result is very similar to the results that were obtained for the single component systems (Figs. 5B and 6B). The reason for the outlet concentration of ethanol in Fig. 7 at 175°C and 200°C being higher than that at the inlet is that ethanol is formed from the decomposition of ethyl acetate at these temperatures (cf. Fig. 5B). It should be noticed that the temperature for the complete combustion of the mixture, 275°C, is the same as that which is required for the feed with ethyl acetate and water alone (Fig. 5B). For the combustion of ethanol in humid air, a lower inlet temperature, 250°C, is required (Fig. 6B). However, it is important to keep in mind that complete combustion must be obtained. Otherwise acetaldehyde will be emitted, which is more harmful than any of the inlet compounds. For example, in the Federal Republic of Germany, the legal emission limit is much higher for solvents, 0.15 g/m^3, than for acetaldehyde, 0.02 g/m^3 (48). Also other investigators (5–8) have reported formation of acetaldehyde during the combustion of ethanol over metal oxide catalysts, and Lintz and Wittstock (48, 49) have shown that several partial oxidation products including acetaldehyde may form during the combustion of acetone and butyl acetate over metal oxides. However, the formation of by-products is not restricted to base metal oxide catalysts, because it has also been observed to be the case using precious metal catalysts (5–7, 50, 51). In ethyl acetate oxidation over a Pt/Al_2O_3 catalyst Sawyer and Abraham (11) detected ethanol, acetic acid, and ethyl ether as intermediate products, which were mainly formed at the surface of the Al_2O_3 support. Obviously, it is very important to carefully identify all the compounds being formed during the combustion and to secure that no harmful products are

emitted. Catalytic incineration in stationary applications, compared with the application for alcohol-fuelled vehicles, has the advantage that it is easy to control the inlet temperature to the catalyst and keep the temperature high enough to obtain complete combustion. It is, however, important to be careful during start-up and shut-down of the incinerator and also to be observant of catalyst deactivation.

CONCLUSIONS

We have found that CeO_x is well dispersed on TiO_2 up to a loading in-between 3 and 12 μmol Ce/m^2 surface area of the support. The Ce-doped titania surface is good as support for CuO_x, and the cerium improves the stability of the titania towards sintering and enhances the activity of the copper species being active for the combustion of CO, ethanol, and ethyl acetate. The improved stability is due to decoration of the titania surface with a limited amount of cerium ions. TPR results reveal interaction of cerium with both the titania and the copper oxide. The interaction between cerium and copper results in improved reducibility of the active copper oxide species, which explains the improved catalytic activity. At a copper loading of 12 μmol/m^2 surface area of the support, corresponding to a theoretical monolayer, characterisation with XRD, FT-Raman, TPR, and XPS indicates that the dispersed copper species forms patches or a bidimensional layer which interacts with the surface of the support. When the content of cerium and copper is low, other types of dispersed copper species are present, which possibly are monomers or dimers. The copper species are predominantly Cu^{2+} species.

Acetaldehyde is an intermediate in the combustion of both ethanol and ethyl acetate over Cu-Ce-Ti-O catalysts. Since acetaldehyde is more harmful than any of the reactants and also is photochemically active, it is important in applications to take measures to assure that the combustion is complete. Cu-Ce-Ti-O catalysts show good performance for feeds both without and with water vapour. Although the concentration of intermediates are affected by the addition of water, there is little effect on the temperature required for obtaining complete conversion to carbon dioxide and water.

ACKNOWLEDGMENTS

Mrs. Birgitta Svensson is gratefully acknowledged for assisting with the BET analyses and we are grateful to the Norton Company for providing the titania supports.

REFERENCES

1. Wiederkehr, P., *in* "Characterization and Control of Odours and VOC in the Process Industries" (S. Vigneron, J. Hermia, and J. Chaouki, Eds.), Studies in Environmental Science, Vol. 61, p. 11. Elsevier, Amsterdam, 1994.
2. Bouscaren, R., Allemand, N., and Dang, Q. C., *in* "Characterization and Control of Odours and VOC in the Process Industries" (S. Vigneron, J. Hermia, and J. Chaouki, Eds.), Studies in Environmental Science, Vol. 61, p. 37. Elsevier, Amsterdam, 1994.
3. Noordally, E., Richmond, J. R., and Tahir, S. F., *Catal. Today* **17**, 359 (1993).
4. The Swedish Environmental Protection Agency, "Flyktiga organiska ämnen och kväveoxider" ("Volatile Organic Compounds and Nitrogen Oxides"), SNV Report 4532, 1996.
5. McCabe, R. W., and Mitchell, P. J., *Ind. Eng. Chem. Prod. Res. Dev.* **23**, 196 (1984).
6. McCabe, R. W., and Mitchell, P. J., *Ind. Eng. Chem. Prod. Res. Dev.* **22**, 212 (1983).
7. Yu Yao, Y.-F., *Ind. Eng. Chem. Process Des. Dev.* **23**, 60 (1984).
8. Rajesh, H., and Ozkan, U. S., *Ind. Eng. Chem. Res.* **32**, 1622 (1993).
9. Pettersson, L. J., Järås, S. G., Andersson, S., and Marsh, P., *in* "Catalysis and Automotive Pollution Control III" (A. Frennet and J.-M. Bastin, Eds.), Studies in Surface Science and Catalysis, Vol. 96, p. 855. Elsevier, Amsterdam, 1995.
10. Chen, J., Heck, R. M., and Farrauto, J., *Catal. Today* **11**, 517 (1992).
11. Sawyer, J. E., and Abraham, M. A., *Ind. Eng. Chem. Res.* **33**, 2084 (1994).
12. Spivey, J. J., *Ind. Eng. Chem. Res.* **26**, 2165 (1987).
13. Larsson, P.-O., Andersson, A., Wallenberg, L. R., and Svensson, B., *J. Catal.* **163**, 279 (1996).
14. Kumar, K.-N. P., *Appl. Catal. A* **119**, 163 (1994).
15. Yuan, S., Mériaudeau, P., and Perrichon, V., *Appl. Catal. B* **3**, 319 (1994).
16. Schaper, H., Doesburg, E. B. M., and van Reijen, L. L., *Appl. Catal.* **7**, 211 (1983).
17. Burtin, P., Brunelle, J. P., Pijolat, M., and Soustelle, M., *Appl. Catal.* **34**, 225 (1987).
18. Barret, E. P., Joyner, L. G., and Halenda, P. H., *J. Am. Chem. Soc.* **73**, 373 (1951).
19. JCPDS International Centre for Diffraction Data, "Powder Diffraction File," Swarthmore, PA, 1991.
20. Pfefferle, L. D., and Pfefferle, W. C., *Catal. Rev. Sci. Eng.* **29**, 219 (1987).
21. Schraml-Marth, M., Wokaun, A., and Baiker, A., *Fresenius J. Anal. Chem.* **341**, 87 (1991).
22. Shyu, J. Z., Weber, W. H., and Gandhi, H. S., *J. Phys. Chem.* **92**, 4964 (1988).
23. Reimann, K., and Syassen, K., *Solid State Commun.* **76**, 137 (1990).
24. Le Normand, F., Hilaire, L., Kili, K., Krill, G., and Maire, G., *J. Phys. Chem.* **92**, 2561 (1988).
25. Wrobel, G., Lamonier, C., Bennani, A., D'Huysser, A., and Aboukaïs, A., *J. Chem. Soc. Faraday Trans.* **92**, 2001 (1996).
26. Laachir, A., Perrichon, V., Badri, A., Lamotte, J., Catherine, E., Lavalley, J. C., El Fallah, J., Hilaire, L., le Normand, F., Quéméré, E., Sauvion, G. N., and Touret, O., *J. Chem. Soc. Faraday Trans.* **87**, 1601 (1991).
27. Otamiri, J. C., Andersson, S. L. T., and Andersson, A., *Appl. Catal.* **65**, 159 (1990).
28. Nogier, J. Ph., and Delamar, M., *Catal. Today* **20**, 109 (1994).
29. Trovarelli, A., *Catal. Rev.* **38**, 439 (1996).
30. Larsson, P.-O., Berggren, H., Andersson, A., and Augustsson, O., *Catal. Today* **35**, 137 (1997).
31. Amores, J. M. G., Escribano, V. S., Busca, G., and Lorenzelli, V., *J. Mater. Chem.* **4**, 965 (1994).
32. Shannon, R. D., and Pask, J. A., *J. Am. Ceram. Soc.* **48**, 391 (1965).
33. Oliveri, G., Ramis, G., Busca, G., and Escribano, V. S., *J. Mater. Chem.* **3**, 1239 (1993).
34. Pauling, L., "The Nature of the Chemical Bond," 3rd ed., Cornell Univ. Press, New York, 1960.

35. Holzapfel, V. H., and Sieler, J., *Z. Anorg. Allg. Chemie* **343**, 174 (1966).
36. Yao, H. C., and Yao, Y. F., *J. Catal.* **86**, 254 (1984).
37. Wöllner, A., Lange, F., Schmelz, H., and Knözinger, H., *Appl. Catal. A* **94**, 181 (1993).
38. Bond, G. C., Namijo, S. N., and Wakeman, J. S., *J. Mol. Catal.* **64**, 305 (1991).
39. Talipova, Sh. A., and Vorobiev, V. N., *React. Kinet. Catal. Lett.* **32**, 469 (1986).
40. Frost, D. C., Ishitani, A., and McDowell, C. A., *Mol. Phys.* **24**, 861 (1972).
41. Mestl, G., and Knözinger, H., *in* "Handbook of Heterogeneous Catalysis" (G. Ertl, H. Knözinger, and J. Weitkamp, Eds.), Vol. 2, p. 539. VCH, Weinheim, 1997.
42. Busca, G., and Zecchina, A., *Catal. Today* **20**, 61 (1994).
43. Luo, M.-F., Zhong, Y.-J., Yuan, X.-X., and Zheng, X.-M., *Appl. Catal. A* **162**, 121 (1997).
44. Abi-Aad, E., Bennani, A., Bonnelle, J.-P., and Aboukaïs, A., *J. Chem. Soc. Faraday Trans* **91**, 99 (1995).
45. Liu, W., and Flytzani-Stephanopoulos, M., *J. Catal.* **153**, 304 (1995).
46. Liu, W., and Flytzani-Stephanopoulos, M., *J. Catal.* **153**, 317 (1995).
47. Zey, E. G., *in* "Kirk-Othmer, Encyclopedia of Chemical Technology" (M. Grayson and D. Eckroth, Eds.), 3rd ed.,Vol. 9, p. 300. Wiley, New York, 1980.
48. Linz, H.-G., and Wittstock, K., *Catal. Today* **27**, 237 (1996).
49. Lintz, H.-G., and Wittstock, K., *Catal. Today* **29**, 457 (1996).
50. Cordi, E. M., and Falconer, J. L., *J. Catal.* **162**, 104 (1996).
51. Papaefthimiou, P., Ioannides, T., and Verykios, X. E., *Appl. Catal. B* **13**, 175 (1997).